Lab on a Chip

PAPER

View Article Online
View Journal | View Issue

Cite this: *Lab Chip*, 2014, **14**, 3556

Cell detachment and label-free cell sorting using modulated surface acoustic waves (SAWs) in droplet-based microfluidics

Adrien Bussonnière,[a] Yannick Miron,[b] Michaël Baudoin,*[a] Olivier Bou Matar,[a] Michel Grandbois,[b] Paul Charette*[cd] and Alan Renaudin*[cd]

Received 28th May 2014,
Accepted 30th June 2014

DOI: 10.1039/c4lc00625a

www.rsc.org/loc

We present a droplet-based surface acoustic wave (SAW) system designed to viably detach biological cells from a surface and sort cell types based on differences in adhesion strength (adhesion contrast) without the need to label cells with molecular markers. The system uses modulated SAW to generate pulsatile flows in the droplets and efficiently detach the cells, thereby minimizing the SAW excitation power and exposure time. As a proof of principle, the system shows efficient sorting of HEK 293 from A7r5 cells based on adhesion contrast. Results are obtained in minutes with sorting purity and efficiency reaching 97% and 95%, respectively.

1. Introduction

Cell sorting is critical for many biological and biomedical applications such as cell biology, biomedical engineering, diagnostics and therapeutics. Indeed, numerous biological analyses are based on the separation of different cell types harvested from a raw heterogeneous sample such as whole blood. Fluorescence-activated cell sorting (FACS)[1] and magnetic-activated cell sorting (MACS)[2] are well-established methods for cell and particle sorting and are known for their high throughput and specificity. Both methods, however, require pre-processing to tag cells with markers, an important time and cost expense for some applications.

In contrast, by making use of the differences in the intrinsic physical properties of cells (size, density, adhesion strength, stiffness, electrical and optical polarizability), label-free sorting methods do not require molecular tagging. Compared to FACS and MACS, however, the specificity of label-free methods is often limited owing to insufficient contrast in physical properties, thereby restricting their widespread use. As with tagging-based systems, label-free cell-sorting methods have been implemented in microfluidic devices[3] using techniques such as deterministic lateral displacement,[4] hydrodynamic filtration,[5] dielectrophoresis (DEP),[6,7] optical lattices,[8,9] stiffness separation,[10,11] acoustophoresis[12,13] and adhesion-based sorting.[14–16] In some cases, such as sorting based on adhesion to the substrate, performance was improved by surface nanostructuring[15] and bio-functionalization[16] which enhance adhesion contrast between cell types.

In addition to sorting, the dynamics of cell detachment from solid surfaces is of interest in and of itself, either to harvest cells or to study the mechanisms of cell adhesion to surfaces. Cell dissociation and detachment from a solid substrate are normally achieved by cleaving bonding proteins with trypsin.[17] This process is quite aggressive as cells can be damaged if left exposed to trypsin for too long and a post-treatment rinsing step is required. In contrast, cell detachment based on microfluidic effects alone requires no external agents or rising. Cell detachment under constant fluid shear stresses has been demonstrated using spinning discs,[18] flow chambers[19] and, more recently, using surface acoustic wave (SAW)-actuated flow.[20,21]

The miniaturization of cell-manipulation methods has led to their integration into lab-on-chip (LOC) platforms, where cell detachment and sorting have been widely investigated in flow-based microchannel formats.[19,22,23] Comparatively few studies,[24–27] however, have explored cell separation or detachment in droplet-based microfluidics as in digital microfluidics (DMF).[28] Indeed, the physics of microfluidics in droplets is completely distinct from flow-through closed-channel systems. Microfluidics properties such as bulk and surface modes of vibration, which are unique to droplet-based systems, can be exploited to great effect. In general,

[a] *LIA LEMAC/LICS, Institut d'Eléctronique de Microélectronique et de Nanotechnologies (IEMN) UMR CNRS 8520, Université Lille 1 and EC Lille, Avenue Poincaré, BP 60069, 59652 Villeneuve d'Ascq, France. E-mail: michael.baudoin@univ-lille1.fr*

[b] *Département de Pharmacologie, Falculté de médecine et des sciences de la santé, Université de Sherbrooke, 3001, 12e Avenue Nord Sherbrooke, Sherbrooke, Québec J1H 5N4, Canada*

[c] *Laboratoire Nanotechnologies Nanosystèmes (LN2)- CNRS UMI-3463, Université de Sherbrooke, 3000 Boulevard Université, J1K OA5, Québec, Canada. E-mail: Alan.Renaudin@USherbrooke.ca, Paul.G.Charette@usherbrooke.ca; Fax: +1 (819) 821 7937; Tel: +1 (819) 821 8000 x65788*

[d] *Institut Interdisciplinaire d'Innovation Technologique (3IT), Université de Sherbrooke, 3000 Boulevard Université, J1K OA5, Québec, Canada*

unlike continuous flow systems which are often optimized for high-volume cell sorting, droplet-based systems are best suited for studies of cell properties in small populations of cells, such as cell adhesion modulation mechanisms which are highly complex and of wide-ranging interest.[29,30]

Droplet actuation in DMF is generally accomplished with surface acoustic waves (SAWs),[31–33] electrowetting on dielectrics (EWOD)[34] or dielectrophoresis (DEP).[35] SAW-based DMF has been used in a range of biological applications[36–38] to implement functions as diverse as mixing,[39] droplet displacement,[40,41] and atomization[42] as well as for particle and cell manipulation.[43] Although EWOD has been used successfully to manipulate cells,[25] large or strongly-adhering cells are difficult to detach and/or transport with the relatively weak electrowetting forces exerted by EWOD. In the case of DEP, the oscillatory forces applied to the cell are subject to changes in the physical composition of the membrane,[44] which may or may not be desirable depending on the nature of the experiment. The strong electrical fields involved in DEP also have the potential to alter cell membrane characteristics.[45]

Recently,[46] we presented preliminary results on the use of SAW-based fluid actuation in droplets to detach biological cells from a surface. We showed that under continuous SAW excitation, fully confluent cell layers could be detached *en masse* at sufficiently high SAW power, whereas isolated cells were very resistant to detachment, even at power levels above the threshold for cell viability.[47] In a previous publication, we showed that the acoustic power required to move or deform droplets with SAW can be significantly reduced by using modulated rather than continuous excitation.[48] Based on this work, we demonstrate here that modulated SAW can be used to viably detach cells from a surface and sort cells based on adhesion contrast, without the need for labeling. The experimental results presented show that two distinct cell types can be separated with a final purity of up to 97% and an efficiency greater than 95%. Results are achieved with characteristic processing times on the order of one minute without adversely affecting cell viability or requiring the cell layer to be fully confluent.

2. Methods and materials

2.1. Apparatus set-up and experimental procedure

Experiments were run on cells adhered to the surface of a $LiNbO_3$ substrate and immersed in 20 μl droplets of phosphate-buffered saline (PBS) solution.

Rayleigh-type SAWs were generated at the surface of the $LiNbO_3$ substrate by applying a 17.1 MHz sinusoidal radio frequency (RF) excitation to interdigitated transducer (IDT) thin-film metal electrodes. The excitation frequency was selected to maximize the energy transmission from the substrate surface to the liquid. The IDTs were designed as "electrode width controlled single-phase unidirectional transducers" (EWC-SPUDT),[49] a configuration that ensures that the acoustic energy is directed solely in the forward direction. The excitation signal was supplied by an RF generator (Agilent, model N9310a) and amplified to 30 dBm using an RF amplifier (Empower, model BBM0D3FEL).

Once transmitted to the fluid, the acoustic waves induce interface stresses and internal flow, resulting in deformations of the droplet-free surface due to two types of nonlinear effects: acoustic radiation pressure and acoustic streaming.[40] As explained below, cyclic droplet deformations were induced by switching the SAW excitation on and off with an appropriate period and duty cycle, resulting in large shear stresses in the fluid causing cells to detach.

An 8 × 8 mm^2 "cell-attachment zone" was defined by markers patterned onto the $LiNbO_3$ substrates. The devices were mounted under a phase contrast microscope (Motic, model AE 30/31) with a 10× objective to focus on the cell layer (2 mm diameter field of view). A high-speed 10 bit CMOS camera (PCO, model pco.1200hs) was used to capture the video of cell detachment. The set-up is depicted in Fig. 1.

Image sequences recorded by the camera were processed using ImageJ (NIH, rsbweb.nih.gov/ij) and cell populations were counted using the ImageJ cell counting tool. The two cell types used in the experiments could be easily distinguished in the images based on differences in their morphological characteristics. Following each experiment, short-term cell viability assays were performed by trypan blue exclusion.

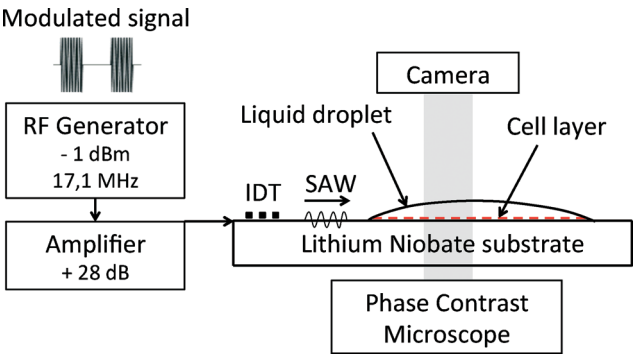

Fig. 1 Schematic diagram of the set-up showing the cell layer (red dashed line) immersed in a 20 μl PBS droplet atop a $LiNbO_3$ piezoelectric substrate. The diagram also shows the interdigitated transducers (IDTs), RF amplifier and signal generator used for Rayleigh type SAW generation. Cell visualization is achieved using a phase contrast microscope, 10× objective, and a CMOS camera.

2.2 SAW device fabrication

The SAW devices were fabricated from 1 mm thickness *X*-cut *Z*-propagating $LiNbO_3$ wafers (Newlight Photonics). This particular cut was chosen for its efficient electromechanical coupling along both *Y* and *Z* perpendicular propagation directions (K_z = 4.9%, K_y = 3.1%), allowing for two-dimensional droplet actuation if required. Indeed, the K^2 values along the two directions are greater than those of a typical 128° *Y*–*X* cut $LiNbO_3$ crystal (K_x = 5.5%, K_y = 1.2%).

The metal IDT electrodes and cell-attachment zone markers were fabricated by photoresist (Shipley S18-13, Microchem) spin-coating on the $LiNbO_3$ wafers, patterning by standard photolithography processes, metal deposition (Ti/Au, 20/200 nm), and lift-off.

2.3. Cell culture and surface preparation

Two cell lines were used in the experiments: adherent vascular smooth muscle cells (A7r5) and human embryonic kidney (HEK 293) cells. These particular cell lines were selected because they have been shown to exhibit surface adhesion strengths comparable to that of cancerous[50] and other normal[51] cell types. Cell adhesion strength, however, is highly dependent on surface preparation specifics. We chose to adhere cells directly to a bare lithium niobate ($LiNbO_3$) substrate, the piezoelectric material most commonly used to generate surface acoustic waves, in order to provide a recognizable point of reference. The adhesion of cells to bare $LiNbO_3$ has been studied by other groups.[52] As shown below, the fluid shear stresses required to detach cells from a bare $LiNbO_3$ surface are in the same range as that reported by others for surface preparations commonly used for cell studies. If required, $LiNbO_3$ can be readily functionalized for specific surface preparations.[53,54] Cells were adhered to the device surfaces either by growing the cells directly on the $LiNbO_3$ substrates in the case of single cell line reference experiments or by incubating the $LiNbO_3$ substrates in a solution of pre-grown resuspended cells in the case of single and dual cell line experiments.

A7r5 and HEK 293 cells were grown separately by seeding in 60 mm petri dishes and cultured in growth medium (DMEM supplemented with 10% heat-inactivated fetal bovine serum, 2 mM L-glutamine, 50 IU mL^{-1} penicillin, 50 μg mL^{-1} streptomycin, Wisent) under an atmosphere of 5% CO_2 at 37 °C for 24 h. For experiments requiring cells to be grown directly onto $LiNbO_3$ surfaces, the $LiNbO_3$ substrates were placed at the bottom of the petri dish for the duration of the incubation time.

For cells not grown directly onto the $LiNbO_3$ substrates, single cell line resuspended cell solutions were prepared by rinsing the cell cultures in PBS, incubating for 5 min in 500 μl of trypsin–EDTA solution at 37 °C, and resuspending in 2 ml of growth medium to stop the trypsin digestion. After 5 min of centrifugation, cells were resuspended in HEPES-buffered salt solution (HBSS) (20 mM HEPES at pH 7.4, 120 mM NaCl, 5.3 mM KCl, 0.8 mM MgSO4, 1.8 mM $CaCl_2$, and 11.1 mM dextrose). Dual cell line resuspended solutions were prepared by combining HEK 293 and A7r5 resuspended solutions in experimentally determined proportions as required for roughly equal numbers of both cell types to adhere to the surface (Fig. 2). $LiNbO_3$ substrates were placed in a petri dish immersed in resuspended cell solutions for incubation times ranging from 15 to 90 min to study various adhesion states.

Following cell adhesion by either of the two methods above, the $LiNbO_3$ substrates were rinsed with PBS, cells outside the attachment zone were dried and mechanically removed, leaving a uniformly distributed 8 × 8 mm^2 adherent cell layer covered by a thin PBS film. A 20 μl droplet of PBS was added atop the attachment zone using a calibrated micropipette prior to experiments. Note that due to adherent cell secretions, the cell-attachment zone was highly hydrophilic and the droplets spread across the square-shaped area with a high contact angle and a flat profile.

3. Results and discussion

3.1. Droplet dynamics and cell–fluid interaction

As stated earlier, the purpose of this work was to investigate the potential of modulated SAW fluid actuation to selectively detach and sort cells in a droplet. Fig. 3a shows a schematic diagram of the PBS fluid droplet atop the 8 × 8 mm^2 droplet positioning zone on the $LiNbO_3$ substrate, in relation to the SAW electrodes (EWC-SPUDT). Cyclic deformations of the droplets between a relaxed state and a deformed state (side-view camera images shown in Fig. 3b, top and bottom, respectively) were induced by switching the SAW signal on (excitation) and off (relaxation) with an appropriate period and duty cycle. During excitation, internal flow and surface deformation are induced by nonlinear acoustic forces. During relaxation, the potential energy stored as capillary surface energy produces a restoring flow in the opposite direction. Optimal values for the period (200 ms), duty cycle (25%), and power (30 dBm) were based on the droplet intrinsic relaxation time, measured experimentally.

The 50 ms SAW excitation bursts displaced the distal liquid–solid contact line (droplet edge furthest from the SAW

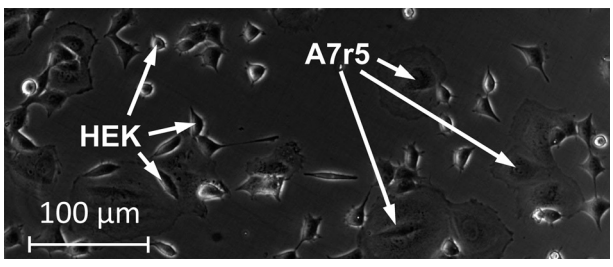

Fig. 2 Photograph of vascular smooth muscle cells (A7r5) and human embryonic kidney (HEK 293) cells adhered to the surface of a $LiNbO_3$ substrate after incubation in a resuspended cell solution at 37 °C. The arrows indicate typical specimens of HEK 293 and A7r5 cells which exhibit significantly different morphological features.

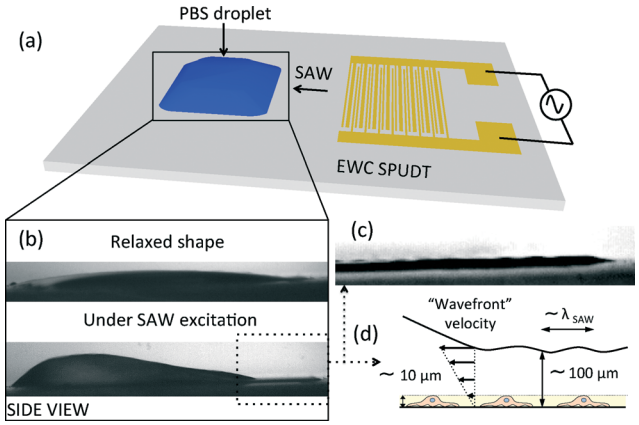

Fig. 3 (a) Schematic diagram of the fluid droplet in its relaxed position spread across the 8 × 8 mm^2 droplet positioning zone atop the $LiNbO_3$ substrate, in relation to the SAW electrodes (EWC-SPUDT); (b) side-view camera images showing the two shape extrema of the droplet during one SAW excitation modulation cycle (ON: 50 ms, OFF: 150 ms). (c) Zoom on the tail section of the drop showing a standing wave pattern. (d) The flow profile of the tail section and characteristic lengths.

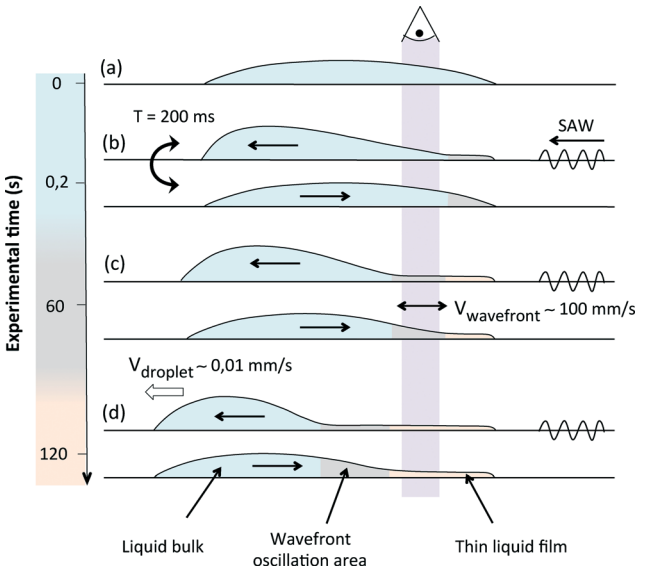

Fig. 4 Schematic diagrams of the different droplet fluid dynamics regimes under modulated SAW actuation (ON: 50 ms, OFF: 150 ms). The vertical bar shows the location of the circular area (2 mm diameter) imaged by the microscope; (a) relaxed shape of the droplet mainly determined by its wetting properties on the cell-covered $LiNbO_3$ substrate; (b) initial shape extrema pair in each excitation/relaxation cycle. (c) After a sufficient number of cycles, a 150 ms relaxation interval between SAW excitation bursts is no longer sufficient to return the droplets to a relaxed symmetric shape of (b). As a result, three distinct fluid dynamics zones can be distinguished: bulk (blue), transient (gray), and thin-film "tail" (orange); (d) eventually, as the droplet spreads sufficiently, the field of view of the camera is confined to the thin-film tail.

electrodes) at a rate of a few microns per cycle while the proximal contact line (droplet edge closest to the SAW electrodes) remained pinned due to the high contact angle hysteresis. As a result, the droplets spread in the direction of SAW propagation at a velocity of ~0.01 mm s^{-1}. As shown in Fig. 4, this expansion elicited three distinct fluidic regimes in the droplets. Since the field of view of the camera (vertical column in Fig. 4) was fixed relative to the spreading droplet, the three fluidic regimes swept sequentially across the field of view and thus could be separated in time in the image sequences.

At the start of the experiments, the expansion was sufficiently small so that the droplets essentially oscillated between the two shape extrema shown schematically in Fig. 4b and in the photographs in Fig. 3b. During SAW excitation (Fig. 4b, top), most of the fluid was displaced in a "bulk" zone at the distal end of the droplet whilst leaving behind a thin film "tail", as previously observed by Rezk *et al.* and Collins *et al.*[55,56] During relaxation, the droplet returned to its relaxed symmetric shape due to surface tension effects (Fig. 4b, bottom).

After a sufficient number of cycles, the distal contact line displacement became significant enough (~0.5 mm) that a 150 ms relaxation interval between SAW excitation bursts was no longer sufficient to return the droplets to a relaxed symmetric shape. As a result, three distinct fluid dynamics regimes (Fig. 4c) could be distinguished in the droplets. As before, the extrema were (1) the bulk (shaded blue area), in which shear stresses result from a combination of large scale vortices induced by Eckart streaming[57] and small-scale vortices due to Rayleigh and Schlichting streaming[58,59] near the viscous boundary layer, and (2) the thin film tail (shaded orange area), in which Schlichting and Rayleigh streaming generated by a standing wave (as evidenced by periodic patterns in Fig. 3c) is dominant.[55] In between the two, a transient zone appeared (gray shaded area), swept by a strong oscillating "wavefront" resulting from the fluid transitions to and from the extrema.

As shown in the experimental results below, the rate of cell detachment from the surface was consistently highest in the transient zone. Eventually, as the droplets spread sufficiently, cells in the field of view of the camera were confined to the thin film tail (Fig. 4d, shaded orange area).

3.2. Magnitude of the shear stresses and unsteady forces in the transient zone

Shear stresses in the fluid acting on the cells were estimated from the image sequences in the transient zone. Assuming no-slip boundary conditions (null velocity at the liquid–solid interface), the vertical shear stress, τ, in the fluid can be linearly approximated (Fig. 3d) by:

$$\tau = \mu \frac{\partial v}{\partial y} \sim \mu \frac{V_{\text{wavefront}}}{h}, \quad (1)$$

where y is the distance perpendicular to the surface, v is the fluid velocity in the direction parallel to the surface at height y, and μ is the dynamic viscosity of the medium (10^{-3} m^2 s^{-1} for PBS at 20 °C). In this formula, $V_{\text{wavefront}}$ and h denote the surface velocity and the height of the thin film, respectively,

estimated from a side-view image sequence (h ~ 100 μm). Under SAW excitation, the "forward" wavefront velocity was about 100 mm s^{-1}, resulting in an estimated vertical shear stress of 1 Pa. When SAW excitation was turned off, the "backward" wavefront velocity was much lower (~10 mm s^{-1}), resulting in an estimated shear stress of 0.1 Pa. For comparison, values of shear stresses reported in the literature to detach cells from treated and untreated surfaces with flow-based systems typically lie between 0.01 and 10 Pa.[16,19,21,60]

In addition to viscous stresses, the pulsatile flow also induces so-called unsteady forces (added mass). The relative magnitudes of viscous and unsteady forces can be quantified by the dimensionless Womersley number $\mathrm{Wo} = \frac{\omega \rho h^2}{\mu}$. In our experiments, Wo was typically ~0.5, meaning that unsteady forces likely also played an important role in cell detachment.

3.3. Cell detachment with a single cell line (HEK 293)

We first investigated the dynamics of cell detachment using our proposed method in experiments with a single cell line (HEK 293). The experiments sought to compare detachment behaviors with substrates prepared using the two protocols described earlier: (1) cells adhered directly to the $LiNbO_3$ substrates after 24 h incubation and (2) $LiNbO_3$ substrates incubated in a solution of resuspended cells (an incubation period of 60 min in this case). In the experiments, ~300 cells were typically adhered initially to the surface in the field of view of the camera.

Because the dynamics of cell detachment from a surface will vary greatly depending on particular conditions, experimental results should be compared in terms of normalized parameters. At a constant rate of detachment, the number of adhered cells will decrease by the same fraction over a time interval of fixed length at any point during the detachment process. As a result, the number of cells adhered to the surface as a function of time, $N(t)$, will follow a decaying exponential profile, $N(t) = N_0 e^{-\sigma t}$, where N_0 is the initial number of attached cells and σ is a detachment rate parameter. Cell detachment dynamics is characterized here in terms of their normalized rate of detachment from the surface, $R(t)$:

$$R(t) = -\frac{1}{N(t)}\frac{\mathrm{d}N(t)}{\mathrm{d}t}. \quad (2)$$

The calculation of $R(t)$ is therefore equivalent to estimating the instantaneous value of the detachment rate parameter, σ, at time t.

Fig. 5 shows the measurements of the fraction of adhered cells over time and the calculated normalized detachment rates under cyclic SAW actuation for experiments with HEK 293 cells prepared with the two adhesion protocols (top: direct to $LiNbO_3$; bottom: incubation in resuspended cells). The three fluid dynamics regimes (bulk, transient and tail) are highlighted by different background colors.

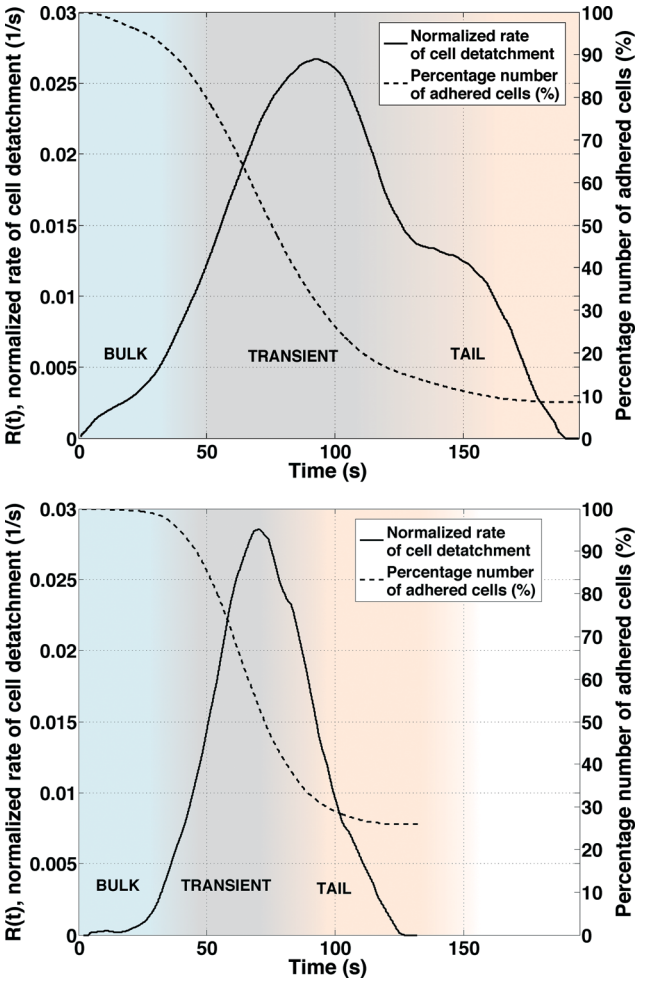

Fig. 5 Normalized detachment rate and percentage of adhered cells over time under cyclic SAW actuation. Top: result from a typical experiment with HEK 293 cells adhered directly to a $LiNbO_3$ substrate after 24 h incubation; bottom: result from a typical experiment with HEK 293 cells adhered to the substrate after incubation in a solution of resuspended cells for 60 min.

Transitions between successive regimes were determined by observing the image sequence where the top of the wavefront in the transient zone could be clearly seen. The uncertainty on estimations of the transition times was on the order of ±5 s. The purpose of these experiments was to explore the relative differences in detachment kinetics between the three fluidic regimes and to extract order of magnitude information if possible about the dynamics. Indeed, a much broader range of experimental conditions would be required to form any kind of quantitative conclusion specific to these particular cell lines.

The results in Fig. 5 clearly show that the cell detachment rate is highest in the transient zone. The two graphs show similar maximum rates of detachment, indicating that both cell adhesion methods can yield similar adhesion strengths to the surface (assuming that detachment rate is an indication of adhesion strength). The inverse of the maximum normalized detachment rate, $1/\max(R(t))$, can be considered as

the "characteristic time" of the system under maximum efficiency, that is to say, the time taken for the number of adhered cells to fall to $(1/e)N_0$ at the maximum rate of detachment. As shown in Fig. 5, this value is ~35 s in both cases. The effect of the duration of the transient regime is also interesting to consider. In Fig. 5 (top), the transient regime is longer (~63 s) resulting in a higher detachment efficacy (>10% residual adhered cells), whereas in Fig. 5 (bottom), due to faster spreading of the droplet, the transient regime is shorter (~46 s) resulting in a lower detachment efficacy (~25% residual adhered cells). In both cases, the majority of cells are detached in minutes, which compares very favorably with the results from other methods.[21,22]

3.4. Cell detachment with dual cell lines (sorting)

We next investigated the selective detachment (sorting) of cell types based on adhesion contrast. $LiNbO_3$ substrates were prepared by incubation in a dual cell solution of resuspended cell lines (A7r5 and HEK293) in a range of incubation periods: 15, 25 and 60 min. Cell sorting performance was characterized by 2 parameters, "purity" and "efficiency", calculated once the system had reached equilibrium, *i.e.* when the number of adhered cells no longer changes (~2 min typically):

$$\text{Purity} = \frac{\%\ \text{HEK 293}_{\text{detached}}}{\%\ \text{HEK 293}_{\text{detached}} + \%\ \text{A7r5}_{\text{detached}}}. \quad (3)$$

$$\text{Efficiency} = \%\ \text{HEK 293}_{\text{detached}}. \quad (4)$$

Fig. 6a shows calculations of cell sorting purity for the three different incubation times. Interestingly, results indicate that purity increases with incubation time. We speculate that this behavior arises because (1) cells require a certain time to achieve complete adhesion and thereby maximizing adhesion contrast between cell types, and (2) it is possible that excretion of the extracellular matrix proteins by A7r5 cells negatively modulates HEK 293 adhesion. Indeed, adhesion modulation by competing species has been observed by other groups, such as the improvement of cancer cell (MCF7) adhesion in the presence of human breast epithelial cells (MCF10A).[15] In all cases, sorting efficiency was greater than 90% (Fig. 6b).

Once detached, cells remained resuspended in the droplets. Short-term viability assays were performed after experiments both with SAW excitation and without SAW as a negative control. Results indicated that SAW excitation only slightly affected the viability (apoptosis rate below 5%).

4. Conclusions

In this paper, we propose a method to selectively and viably detach cells from a solid substrate in fluid droplets using modulated surface acoustic waves (SAWs). Experiments were designed to study the effects of different fluid dynamics regimes by using a fixed imaging field of view with respect to droplet expansion under SAW actuation. Results show that the cell detachment rate is highest in the middle regime, termed "transient regime", where viscous shear stresses are estimated to be of the order of 1 Pa.

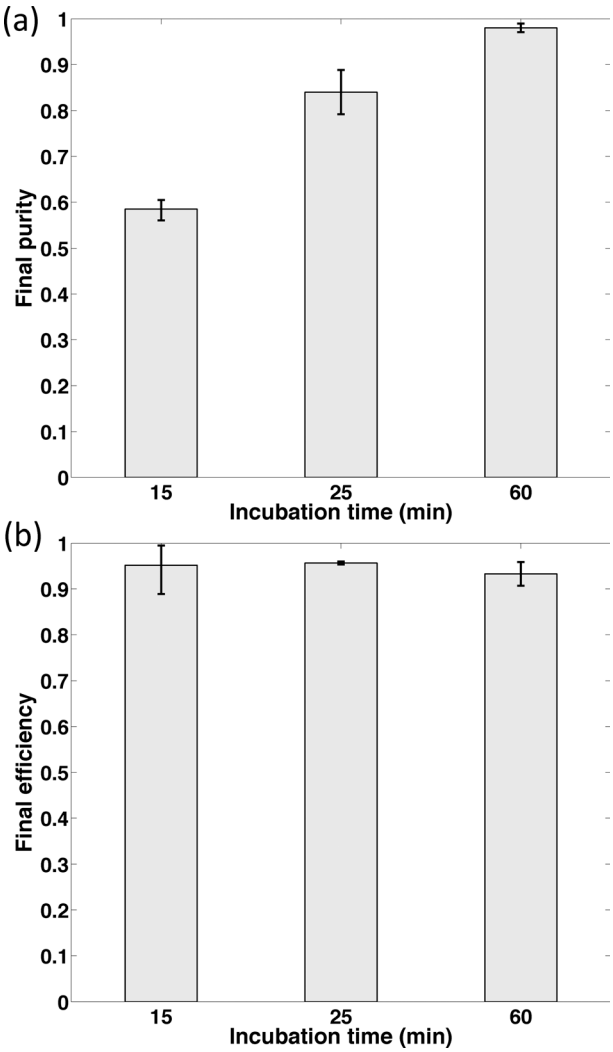

Fig. 6 Cell sorting purity (a) and efficiency (b) for LiNbO3 substrates prepared by incubation in dual cell line resuspended solutions (A7r5 and HEK 293) for a range of incubation periods: 15, 25 and 60 min.

Under the chosen SAW modulation protocol, HEK 293 and A7R5 cells adhered to bare $LiNbO_3$ surfaces were successfully sorted based on adhesion contrast. Results show that cells were detached in the order of minutes and the contrast in adhesion strength varies with incubation time. This method could be generalized to other cell lines exhibiting either intrinsic or controlled (*via* surface bio-functionalization) adhesion contrasts. Importantly, cell adhesion strength is highly dependent on surface preparation specifics and adhesion modulation between competing species. Therefore, SAW excitation parameters required to viably detach and sort cell types under different experimental conditions can be expected to vary according to the characteristics of cell lines,

surface preparation, and adhesion modulation between competing cell species. Similarly, sorting purity and efficiency are expected to be highly dependent on particular experimental conditions.

Interestingly, modulated SAW could be combined with EWOD to detach strongly adhered cells and enhance EWOD cell manipulation and sorting performance. Further investigations with a view to optimizing unsteady forces would also be of interest, for example, with bi-lateral SAW excitation.

Acknowledgements

This work was supported by grants from the Natural Sciences and Engineering Research Council of Canada (NSERC), the Créneau Biotech Santé du Projet ACCORD du Ministère des Finances et de l'Économie (MFEQ) du Québec (Canada), the Agence Nationale pour la Recherche ANR-12-BS09-021-02 et 01 (France), the Direction Générale de l'Armement (France) and Région Nord-Pas-de-Calais (France). The authors would like to thank the Institut Interdisciplinaire d'Innovation Technologique (3IT) at the Université de Sherbrooke (Canada) for technical support.

References

1 L. A. Herzenberg, R. G. Sweet and L. A. Herenberg, *Sci. Am.*, 1976, **234**, 108–117.
2 S. Miltenyi, W. Müller, W. Weichel and A. Radbruch, *Cytometry*, 1990, **11**, 231–238.
3 D. R. Gossett, W. M. Weaver, A. J. Mach, S. C. Hur, H. T. K. Tse, W. Lee, H. Amini and D. Di Carlo, *Anal. Bioanal. Chem.*, 2010, **397**, 3249–3267.
4 L. R. Huang, E. C. Cox, R. H. Austin and J. C. Sturm, *Science*, 2004, **304**, 987–990.
5 M. Yamada and M. Seki, *Lab Chip*, 2005, **5**, 1233–1239.
6 F. F. Becker, X. B. Wang, Y. Huang, R. Pethig, J. Vykoukal and P. R. Gascoyne, *Proc. Natl. Acad. Sci. U. S. A.*, 1995, **92**, 860–864.
7 M. D. Vahey and J. Voldman, *Anal. Chem.*, 2008, **80**, 3135–3143.
8 K. D. M. M. P. MacDonald and G. C. Spalding, *Nat. Biotechnol.*, 2003, **426**, 421–424.
9 A. Jonás and P. Zemánek, *Electrophoresis*, 2008, **29**, 4813–4851.
10 R. Carlson, C. Gabel, S. Chan, R. Austin, J. Brody and J. Winkelman, *Phys. Rev. Lett.*, 1997, **79**, 2149–2152.
11 G. Wang, W. Mao, R. Byler, K. Patel, C. Henegar, A. Alexeev and T. Sulchek, *PLoS One*, 2013, **8**, e75901.
12 T. Laurell, F. Petersson and A. Nilsson, *Chem. Soc. Rev.*, 2007, **36**, 492–506.
13 Y. Ai, C. K. Sanders and B. L. Marrone, *Anal. Chem.*, 2013, **85**, 9126–9134.
14 A. Sin, S. K. Murthy, A. Revzin, R. G. Tompkins and M. Toner, *Biotechnol. Bioeng.*, 2005, **91**, 816–826.
15 K. W. Kwon, S. S. Choi, S. H. Lee, B. Kim, S. N. Lee, M. C. Park, P. Kim, S. Y. Hwang and K. Y. Suh, *Lab Chip*, 2007, **7**, 1461–1468.
16 T. F. Didar and M. Tabrizian, *Lab Chip*, 2010, **10**, 3043–3053.
17 W. Kühne, *Verhandlungen des naturhistorisch-medicinischen Vereins zu Heidelberg, new series*, 1877, vol. 1, pp. 194–198.
18 L. Weiss, *Exp. Cell Res.*, 1961, **8**, 141–153.
19 S. Usami, H. H. Chen, Y. Zhao, S. Chien and R. Skalak, *Ann. Biomed. Eng.*, 1993, **21**, 77–83.
20 M. F. Schneider, Z. Guttenberg, S. W. Schneider, K. Sritharan, V. M. Myles, U. Pamukci and A. Wixforth, *ChemPhysChem*, 2008, **9**, 641–645.
21 A. Hartmann, M. Stamp, R. Kmeth, S. Buchegger, B. Stritzker, B. Saldamli, R. Burgkart, M. F. Schneider and A. Wixforth, *Lab Chip*, 2013, **14**, 542–546.
22 H. Lu, L. Y. Koo, W. M. Wang, D. A. Lauffenburger, L. G. Griffith and K. F. Jensen, *Anal. Chem.*, 2004, **76**, 5257–5264.
23 A. Lenshof and T. Laurell, *Chem. Soc. Rev.*, 2010, **39**, 1203–1217.
24 S.-K. Fan, P.-W. Huang, T.-T. Wang and Y.-H. Peng, *Lab Chip*, 2008, **8**, 1325–1331.
25 G. J. Shah, A. T. Ohta, E. P.-Y. Chiou, M. C. Wu and C.-J. C. J. Kim, *Lab Chip*, 2009, **9**, 1732–1739.
26 G. J. Shah, J. L. Veale, Y. Korin, E. F. Reed, H. A. Gritsch and C.-J. C. Kim, *Biomicrofluidics*, 2010, **4**, 44106.
27 J.-C. Baret, O. J. Miller, V. Taly, M. Ryckelynck, A. El-Harrak, L. Frenz, C. Rick, M. L. Samuels, J. B. Hutchison, J. J. Agresti, D. R. Link, D. A. Weitz and A. D. Griffiths, *Lab Chip*, 2009, **9**, 1850–1858.
28 J. Berthier, *Microdrops and Digital Microfluidics*, William Andrews Publications, 1st edn, 2013.
29 J. T. Parsons, A. R. Horwitz and M. A. Schwartz, *Nat. Rev. Mol. Cell Biol.*, 2010, **11**, 633–643.
30 S. Safran, N. Gov, A. Nicolas, U. Schwarz and T. Tlusty, *Phys. A*, 2005, **352**, 171–201.
31 A. Wixforth, C. Strobl, C. Gauer, A. Toegl, J. Scriba and Z. V. Guttenberg, *Anal. Bioanal. Chem.*, 2004, **379**, 982–991.
32 J. Friend and L. Yeo, *Rev. Mod. Phys.*, 2011, **83**, 647–704.
33 L. Y. Yeo and J. R. Friend, *Annu. Rev. Fluid Mech.*, 2014, **46**, 379–406.
34 W. C. Nelson and C.-J. C. Kim, *J. Adhes. Sci. Technol.*, 2012, **26**, 1–25.
35 M. G. Pollack, R. B. Fair and N. Carolina, *Appl. Phys. Lett.*, 2000, **77**, 1725–1726.
36 Z. Guttenberg, H. Muller, H. Habermüller, A. Geisbauer, J. Pipper, J. Felbel, M. Kielpinski, J. Scriba and A. Wixforth, *Lab Chip*, 2005, **5**, 308–317.
37 T. J. Lyford, P. J. Millard and M. P. Cunha, *IEEE Int. Ultrason. Symp.*, 2012, 1216–1219.
38 A. Renaudin, V. Chabot, E. Grondin, V. Aimez and P. G. Charette, *Lab Chip*, 2010, **10**, 111–115.
39 M. Alghane, Y. Q. Fu, B. X. Chen, Y. Li, M. P. Y. Desmulliez and A. J. Walton, *J. Appl. Phys.*, 2012, **112**, 084902.
40 P. Brunet, M. Baudoin, O. B. Matar and F. Zoueshtiagh, *Phys. Rev. E: Stat., Nonlinear, Soft Matter Phys.*, 2010, **81**, 036315.
41 A. Renaudin, P. Tabourier, V. Zhang, J. Camart and C. Druon, *Sens. Actuators, B*, 2006, **113**, 389–397.
42 A. Qi, L. Y. Yeo and J. R. Friend, *Phys. Fluids*, 2008, **20**, 074103.

43 H. Li, J. R. Friend and L. Y. Yeo, *Biomed. Microdevices*, 2007, **9**, 647–656.
44 Z. Gagnon, J. Gordon, S. Sengupta and H.-C. Chang, *Electrophoresis*, 2008, **29**, 2272–2279.
45 S. Sengupta, J. E. Gordon, H.-C. Chang and N. Dame, *Microfluidic Diagnostic Systems for the Rapid Detection and Quantification of Pathogens*, Springer US, 2009, pp. 271–322.
46 A. Bussonnière, A. Renaudin, Y. Miron, M. Grandbois, M. Baudoin and P. Charette, *Proc. Meetings Acoust.*, 2013, **19**, 045018.
47 H. Li, J. Friend, L. Yeo, A. Dasvarma and K. Traianedes, *Biomicrofluidics*, 2009, **3**, 34102.
48 M. Baudoin, P. Brunet, O. Bou Matar and E. Herth, *Appl. Phys. Lett.*, 2012, **100**, 154102.
49 C. Hartmann and B. Abbott, *Proc. - IEEE Ultrason. Symp.*, 1989, 79–89.
50 B. D. Plouffe, M. Radisic and S. K. Murthy, *Lab Chip*, 2008, **8**, 462–472.
51 C. P. Palmer, M. E. Mycielska, H. Burcu, K. Osman, T. Collins, R. Beckerman, R. Perrett, H. Johnson, E. Aydar and M. B. A. Djamgoz, *Eur. Biophys. J.*, 2008, **37**, 359–368.
52 R. Rodaite-Riseviciene, B. Snopok and V. Snitka, *The 7th IEEE International Conference on Nano/Molecular Medicine and Engineering*, 2013, pp. 7–10.
53 S. Seeger, K. Bierbaum, R. Dahint, C. Feng, M. Mantar and M. Grunze, *Preparation and Characterization of Antibody Films on Lithium Niobate Surfaces*, Springer US, 1992, pp. 53–66.
54 J. Bennès, S. Ballandras and F. Chérioux, *Appl. Surf. Sci.*, 2008, **255**, 1796–1800.
55 A. R. Rezk, O. Manor, J. R. Friend and L. Y. Yeo, *Nat. Commun.*, 2012, **3**, 1167.
56 D. J. Collins, O. Manor, A. Winkler, H. Schmidt, J. R. Friend and L. Y. Yeo, *Phys. Rev. E: Stat., Nonlinear, Soft Matter Phys.*, 2012, **86**, 056312.
57 C. Eckart, *Phys. Rev.*, 1948, **73**, 68–76.
58 L. Rayleigh, *Philos. Trans. R. Soc. London*, 1884, **175**, 1–21.
59 H. Schlichting, *Boundary-Layer Theory*, McGraw-Hill, 1968.
60 A. J. García, P. Ducheyne and D. Boettiger, *Biomaterials*, 1997, **18**, 1091–1098.